Lasers in Surgery and Medicine 44:20–25 (2012)

Microwave Thermolysis of Sweat Glands

Jessi E. Johnson, PhD, Kathryn F. O'Shaughnessy, PhD, and Steve Kim, MS*
Miramar Labs, Inc., Sunnyvale, California 94085

Background and Objectives: Hyperhidrosis is a condition that affects a large percentage of the population and has a significant impact on peoples' lives. This report presents a technical overview of a new noninvasive, microwave-based device for creating thermolysis of sweat glands. The fundamental principles of operation of the device are presented, as well as the design and optimization of the device to target the region where the sweat glands reside.
Materials and Methods: An applicator was designed that consists of an array of four waveguide antennas, a cooling system, and a vacuum acquisition system. Initially, the performance of the antenna array was optimized via computer simulation such that microwave absorption was maximized near the dermal/hypodermal interface. Subsequently, hardware was implemented and utilized in pre-clinical testing on a porcine model to optimize the thermal performance and analyze the ability of the system to create thermally affected zones of varying size yet centered on the target region.
Results: Computer simulation results demonstrated absorption profiles at a frequency of 5.8 GHz that had low amounts of absorption at the epidermis and maximal absorption at the dermal/hypodermal interface. The targeted zone was shown to be largely independent of skin thickness. Gross pathological and histological response from pre-clinical testing demonstrated the ability to generate thermally affected zones in the desired target region while providing protection to the upper skin layers.
Conclusions: The results demonstrate that microwave technology is well suited for targeting sweat glands while allowing for protection of both the upper skin layers and the structures beneath the subcutaneous fat. Promising initial results from simulation and pre-clinical testing demonstrate the potential of the device as a noninvasive solution for sweat gland thermolysis. Lasers Surg. Med. 44:20–25, 2012. © 2011 Wiley Periodicals, Inc.

Key words: dermatology; hyperhidrosis; eccrine glands; microwave; thermolysis; noninvasive

INTRODUCTION

Hyperhidrosis is defined as excessive sweating beyond what is physiologically required to regulate body temperature [1]. Although not life-threatening, hyperhidrosis has a significant impact on peoples' lives and is a condition which affects millions of people worldwide [2]. Its impact is comparable to many of the commonly recognized dermatologic disorders such as psoriasis, acne, and vitiligo [3].

A new noninvasive, microwave-based device has been developed to create thermolysis of sweat glands. This article will provide a technical overview of the device and present some of the device's fundamental principles of operation. A description of the target anatomy, basics of microwave-based therapeutic techniques, and the device configuration will be shown. Computer simulations utilized to design the microwave absorption pattern of the device will also be presented, followed by pre-clinical studies that assessed and optimized the location and size of thermally affected zones created by the device.

MATERIALS AND METHODS

Microwave Energy as a Thermal Treatment Modality

Microwave energy has been under investigation for decades as a modality for medical treatment. Early conceptual work for microwave-based thermal therapy has been reported as early as the 1930s [4,5] and practical hardware development and experimentation in this area began as early as 1946 [6]. Since this early work, research has been extensive and technology has been developed for use in medical fields such as oncology, urology, cardiology, and general surgery [4,7–12]. However, despite this work, microwave technology is less familiar to the medical community than other modalities such as lasers, radio frequency (RF), and ultrasound devices. A brief overview of some of the fundamental principles of microwave energy in relation to medical devices is presented below.

A microwave is typically defined as an electromagnetic signal having a frequency of between 300 MHz and 300 GHz, with a corresponding free-space wavelength of 1 m down to 1 mm [13]. This frequency range lends itself to coupling energy into the body utilizing radiated energy rather than coupling via direct contact or by capacitive (or inductive) coupling as utilized in RF devices [10]. Microwave-based therapeutic medical devices

The authors are all employees of Miramar Labs, Inc., the company developing the technology described in this work.

*Corresponding to: Steve Kim, MS, Miramar Labs, Inc., Sunnyvale, CA 94085. E-mail: skim@miramarlabs.com

Accepted 13 October 2011
Published online in Wiley Online Library (wileyonlinelibrary.com).
DOI 10.1002/lsm.21142

generally consist of an antenna that converts high frequency currents (produced by a microwave generator) into a propagating electromagnetic signal that is transmitted into the body to produce a desired absorption pattern in tissue. The absorption in tissue leads to the process of dielectric heating, a different phenomenon than generating heat via resistance to the flow of free electrons (as in RF devices). At a molecular level, microwave dielectric heating consists of the rapidly changing electric field induced by a microwave signal acting upon dipole moments within the water molecules present in tissue. Molecules are excited by the microwave field, resulting in frictional forces leading to heating [14].

Target Anatomy

It is generally accepted that there are two types of sweat glands that exist: eccrine and apocrine glands. The eccrine glands secrete a clear, nonodorous sweat, whose primary function is thermoregulation of body temperature; these glands are distributed all over the body. The apocrine glands secrete a milky sweat, where the bacterial breakdown of this sweat causes the unique body odor; these glands are primarily found in the axillae and genital region. Both of these glands reside near the dermal/hypodermal interface [15].

Device Configuration and Design

Figure 1 shows a diagram of the antenna array, cooling system components, and the tissue model utilized in the development of the microwave applicator. Microwave energy from a high-power generator is fed into a metal-plated waveguide structure via a coaxial probe as shown in the figure. The probe excites a propagating microwave signal in the waveguide which travels down the structure to an open face with no metal. This open face forms a radiating aperture that allows the transmission of energy out of the waveguide structure, through the cooling system and into tissue. The cooling system is formed from a circulating layer of water and a ceramic cooling plate and serves to prevent thermal damage to the superficial layers of the skin, while allowing therapeutic heat to develop in the deeper target tissue. The applicator also includes a vacuum acquisition system, which is represented in Figure 1 by the "lifted" configuration of the skin and fat regions. The vacuum system lifts the skin and underlying fat layers to achieve additional separation of the energy source from underlying fixed tissue structures and physically isolate the target region.

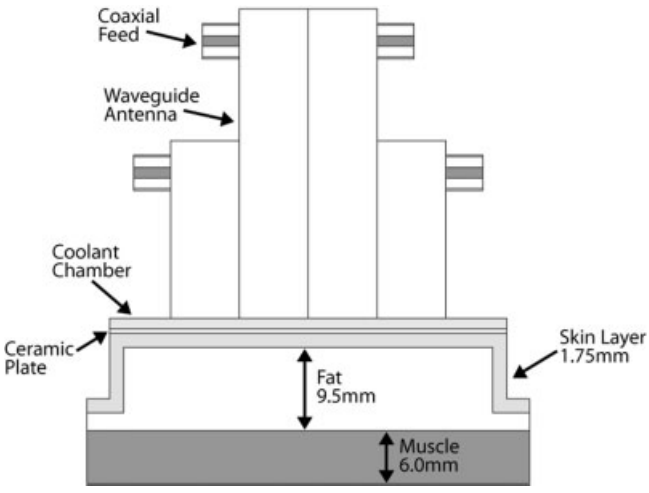

Fig. 1. Geometry of antenna array, cooling system, and tissue model utilized for this study.

The main design goal for this device was to achieve an optimal heating effect in the target tissue. The first step utilized electromagnetic computer simulations using the model described above to determine an optimal antenna geometry and frequency for maximizing microwave absorption near the target region. The computer modeling was followed by hardware implementation and preclinical testing to verify the design and determine optimal energy delivery parameters in terms of heating of the target region as well as protection of the epidermal and upper dermal regions. The details of the electromagnetic simulation and optimization are presented below.

Computer Simulation Setup

An industry-standard three-dimensional microwave simulation tool (CST Microwave Studio, CST of America, Inc., Boston, MA) was utilized to perform the optimization of the electromagnetic response of the system. The model included the four-channel waveguide array, the cooling system and the vacuum acquired tissue model as shown in Figure 1. Using the anatomy of the axilla as an example, the epidermal and dermal layers were modeled as a single 1.75 mm thick slab. The hypodermis was modeled as a 9.5 mm slab of adipose tissue, distended by vacuum, with a layer of underlying muscle tissue 6 mm thick. The microwave properties assumed for the various tissue types are shown in Table 1 for a frequency of 5.8 GHz. The tissue density properties were taken from [16] and are also shown in Table 1. In order to account for patient skin thickness variation, simulations were also conducted with 1.25 and 2.25 mm skin thicknesses. It is of note that the sweat glands themselves, which were shown in preliminary simulation investigations to have minimal affect on absorption pattern, were not explicitly included in the simulations.

As shown in Table 1, there are significant differences in the material properties of the dermal and underlying adipose tissue, with the relative permittivity and microwave conductivity being significantly larger in the dermal tissue. These differences result in two phenomena. The first is that a large reflection of the microwave energy will tend to occur at the dermal/hypodermal interface (in the same manner by which light reflects when striking a material with a different index of refraction than that it is propagating through). Secondly, the large difference in microwave conductivity (which is proportional to the amount of energy absorbed in a material for a given electric field strength) demonstrates that dermal tissue is

TABLE 1. Table of Tissue Properties (Data Taken From [16,25])

Tissue type	Relative permittivity ε_r	Conductivity σ (S/m)	Density ρ (kg/m^3)
Dermal/epidermal	38.62	4.34	1,010
Adipose	4.95	0.29	920
Muscle	49.5	5.44	1,040

The relative permittivity (ε_r) describes the velocity at which the microwave travels through each tissue type, with a large ε_r corresponding to a lower velocity. The conductivity is a measure of how well each tissue type absorbs microwave energy.

more readily subjected to absorption than the adipose layer. These phenomena were utilized to design an antenna geometry to target the region near the dermal/hypodermal interface, as described in further detail below.

Absorption (Specific Absorption Rate, or SAR) profiles were computed by the simulator and utilized to characterize the spatial absorption in tissue and assess the ability of the antennas to treat the target region effectively. SAR is a metric used for treatment zone estimations in microwave hyperthermia because the absorbed energy is converted into heat.

Pre-Clinical Testing

Although the computer simulation results provide accurate estimates of the microwave absorption, they do not account for thermal conduction effects. The constant temperature cooling system protects the superficial region of the skin by inhibiting upward thermal conduction from the peak microwave absorption region. The cooling parameters can also be designed such that the combination of direct microwave heating and thermal conduction creates an optimal therapeutic heating region in the deep dermis and adjacent subdermal tissue. The general concept of designing the combination of microwave absorption pattern and cooling system to create an optimal thermal profile is illustrated in Figure 2. Optimization of the thermal performance was achieved via pre-clinical studies, as described below.

Testing was performed on a porcine model at an Association for the Assessment and Accreditation of Laboratory Animal Care (AAALAC) accredited facility. The porcine model is commonly utilized for dermatological testing, having been used to test many modern laser systems [17–19], wound healing devices and drugs [20], and dermal abrasion systems [18]. It is also widely documented that porcine skin and human skin are similar in morphology and in physiology [21] and their microwave properties have also been shown to be similar [22–24]. The main limitation of the porcine model for this application is that eccrine glands are not present in the target tissue. However, the porcine model has apocrine glands that are similar in size to the human apocrine glands and are located near the dermal–hypodermal interface in the subcutaneous tissue. Since most of the human eccrine glands also reside at the same interface [15], they adequately model the presence of sweat glands for the optimization of thermal performance and provide confidence in the potential to achieve efficacy in humans.

The animal study was conducted in the following manner. The animals were anesthetized and a grid was created on the left and right flank surfaces. Each rectangular area of the grid was a test location for a single treatment. Utilizing a 15°C coolant temperature and an approximate 30 W antenna power per channel, microwave energy levels of 599, 630, and 756 J were utilized. Note that these energy levels represent the total energy spread over seven individual zones treated by a single applicator placement. The 756 J setting represented an example of excessive energy to test the limits of safety and was not considered a clinically viable setting. A minimum of six test locations

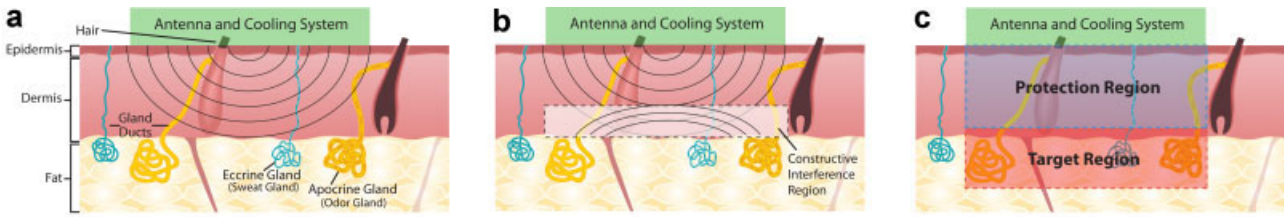

Fig. 2. Diagram demonstrating the basic method by which the sweat gland layer is targeted: (**a**) an incident signal is radiated by the antenna system through the epidermal and dermal layer, (**b**) a significant amount of reflection occurs at the dermal/hypodermal interface, resulting in constructive interference in the dermis near the interface, (**c**) the cooling system protects the epidermal/upper dermal layer and allows thermal conduction from the microwave absorption region to spread to the target zone.

were treated for every energy setting used. Animals were recovered and survived until time-points spanning 1–3 months. Gross pathological examination was utilized to assess the location and size of the thermally affected area, and histopathological analysis was conducted by a veterinary histopathologist to assess the local effects.

RESULTS

Computer Simulation Results

Figure 3 shows a plot of the normalized SAR profile in the plane perpendicular to the skin surface for the optimized design. As the figure shows, power is preferentially absorbed in the dermal layer in the region near the dermal/hypodermal interface. At the skin's surface the SAR is approximately 30% of the maximum, demonstrating the inherent protection of the epidermal and upper dermal layer achieved by the system independent of the cooling which further protects the superficial tissue. The peak SAR occurs in the dermal layer at a distance of 0.25 mm from the dermal/hypodermal interface and quickly drops when transitioning into the hypodermal region. Also, the peak SAR is less than 2% of maximum in the muscle layer, which demonstrates the ability of the system to focus the energy in the target region without causing significant absorption in the underlying structure.

As previously described, a range of skin thicknesses were subsequently simulated for the optimal antenna system geometry to assess the performance over variation in patient skin thickness. Normalized 1D SAR data were calculated and compared to the original result at 1.75 mm, as shown in Figure 4. The figure demonstrates that the peak absorption zone remains in the same location for all simulated skin thicknesses, with some variation in peak energy absorbed.

Pre-Clinical Testing Results

One month post-treatment gross pathological images from the study are shown in Figure 5, with part (a) of the figure showing a baseline untreated area and demonstrating the various tissue regions, and parts (b)–(d) of the figure showing the effects from energy delivery settings of 599, 630, and 756 J respectively. The figure demonstrates how the system was optimized to create a thermal effect consistently in the dermal/hypodermal interface and how the lesion size (range 1–3 mm thickness) was adjustable while still providing protection to the epidermal and upper dermal layers. Figure 6 (a) shows a histological image from the dosage study at the 1 month time-point for the 599 J setting. The majority of the dermal tissue has minimal to no histologic changes in the treatment zone. Inflammation and fibrosis were identified within the deep dermis and subdermal regions where the thermal energy was focused. The sample also shows an apocrine gland with inflammation, suggesting that it was subjected to a significant amount of thermal energy. Figure 6 (b) shows an untreated control sample for comparison. Figure 7 (a) shows another section that was treated at the 630 J setting. Again we notice a similar treatment zone. The boxed area in Figure 7 (a) is shown magnified in Figure 7 (b); the black arrows indicate the necrotic apocrine glands.

In terms of safety, protection of the epidermal and upper dermal layers was evident in the gross and histologic results. No evidence of skin effects such as skin necrosis, blisters, or hyper/hypopigmentation were found for any of the settings. There was a range of edema and erythema in the treatment area that was recorded at each follow-up time point, however these had resolved by the 3-month time-point for the clinically viable settings. The histologic changes were consistent across all of the energy settings; however the area of effect varied.

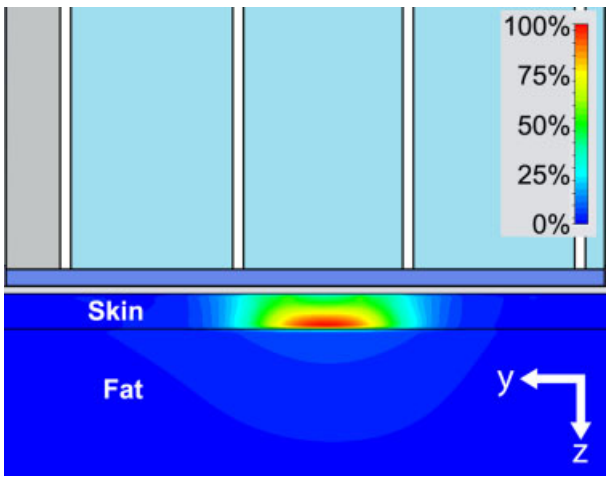

Fig. 3. SAR Plot for the optimized design, skin thickness = 1.75 mm, frequency = 5.8 GHz. The color scale represents the % of maximum SAR at a given point in the 3D model.

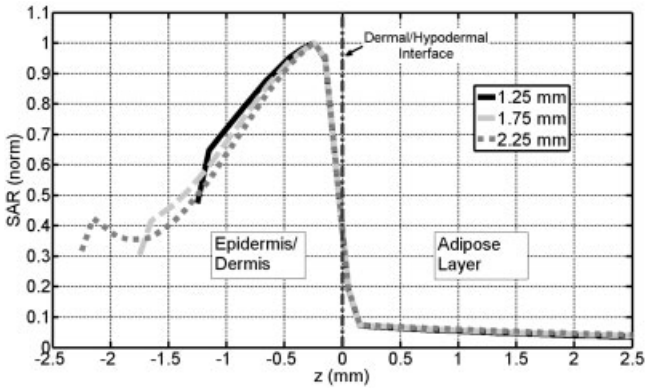

Fig. 4. 1D Normalized SAR profiles through center of waveguide antenna down into tissue, comparison of skin thickness models from 1.25 to 2.25 mm. Plot normalized such that $z = 0$ mm occurs at the dermal/hypodermal interface for each trace. Peak SAR values for each thickness were as follows: 1.25 mm = 1.6×10^5 W/kg, 1.75 mm = 1.2×10^5 W/kg, 2.25 mm = 9.0×10^4 W/kg.

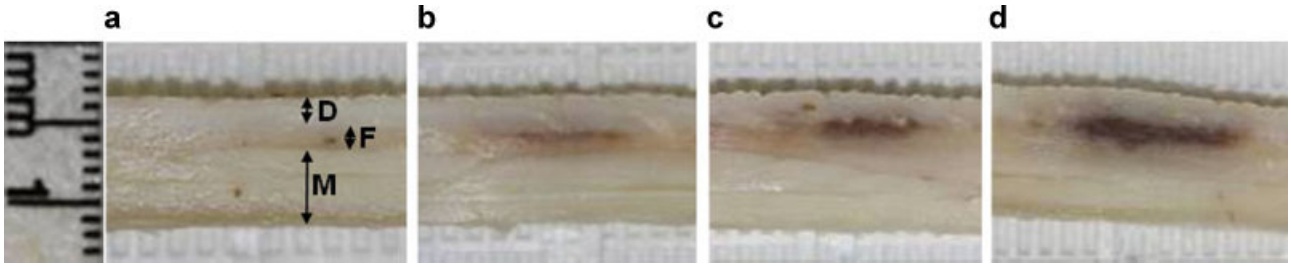

Fig. 5. Gross pathology examination 1 month posttreatment, for tissue treated at various energy levels in porcine model: (**a**) untreated, (**b**) 599 J, (**c**) 630 J, (**d**) 756 J. The dark region (localized hematoma) approximates the area affected by the energy. Note that the baseline untreated case shows the location of the dermal region (D) the fat layer (F) and muscle (M).

DISCUSSION

When delivering microwave energy into tissue, the difference in the dielectric properties between dermal and adipose tissue tend to generate a large amount of reflected energy at the dermal/hypodermal interface. The antenna system was designed to take advantage of this property such that this reflected signal travels back towards the waveguide antenna and creates an optimal interference pattern (i.e., standing wave pattern) with the initial incident signal. The result is constructive interference in the region near the dermal/hypodermal interface and destructive interference near the epidermal layer. The larger conductivity of the dermal tissue results in this constructive interference signal being absorbed mainly on the dermal side of the interface to produce the absorption profile shown in Figure 3.

A great advantage of utilizing the reflected signal to create an optimal interference pattern and corresponding absorption profile is that the reflection occurs at the dermal/hypodermal interface independently of the skin thickness. Thus, as demonstrated in Figure 4, changes in skin thickness do not affect the location of the targeted area. This principal highlights one of the inherent advantages of using this microwave technology for treating sweat glands.

The pre-clinical study showed that delivering energy with the system resulted in thermal injury to a well-defined area at the dermal/hypodermal interface where sweat glands reside. The results also demonstrate the ability of the system to create thermal zones of varying size while maintaining the desired safety profile. The high level of epidermal and upper-dermal protection achievable by the system is also attributable to the ability of the microwave energy to create a peak absorption zone that occurs below these layers. The gross pathological results were verified by the histology, which also clearly showed thermolysis of the apocrine glands.

CONCLUSION

A new noninvasive microwave device for treating sweat glands has been developed. This article has presented a technical overview of the fundamental principles of operation of this device and described how the microwave and thermal performance of the device were optimized for

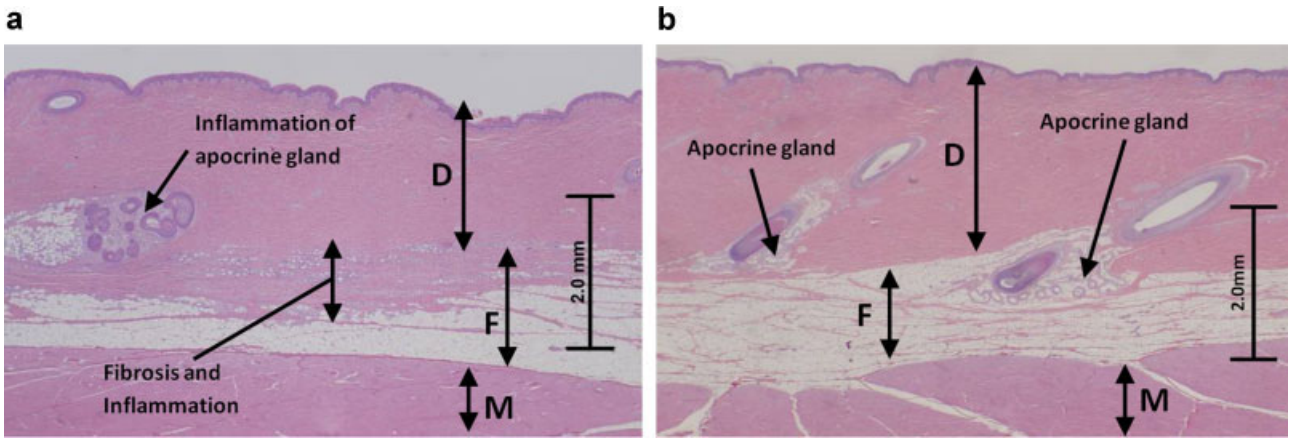

Fig. 6. H&E stained samples in porcine model: (**a**) treated with microwave device at 599 J, (**b**) untreated control. For both cases, dermal region is denoted with a (D), fat layer with an (F), and muscle with an (M).

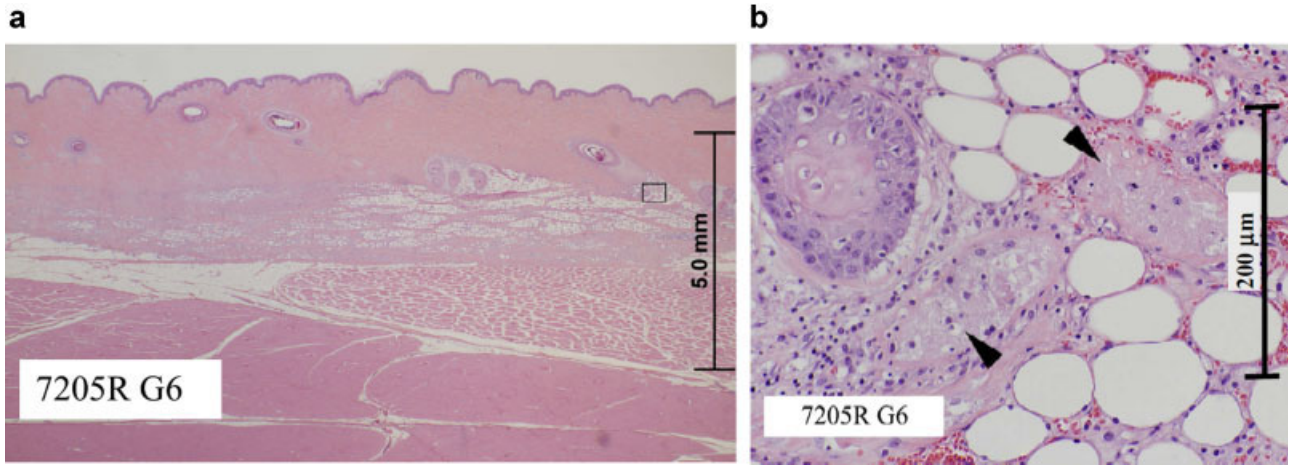

Fig. 7. H&E stained sample in porcine model: (**a**) treated with microwave device at 630 J, (**b**) magnification of part (a); the black arrows indicate the necrotic apocrine glands.

targeting the sweat glands. Clinical investigations of this device should be performed to demonstrate safety and efficacy for the specific indication of use.

REFERENCES

1. Atkins JL, Butler P. Hyperhidrosis: A review of current management. Plast Reconstr Surg 2002;110(1):222–228.
2. Strutton DR, Kowalski JW, Glaser DA, Stang PE. Us prevalence of hyperhidrosis and impact on individuals with axillary hyperhidrosis: Results from a national survey. J Am Acad Dermatol 2004;51(2):241–248.
3. Basra M, Fenech R, Gatt R, Salek M, Finlay A. The dermatology life quality index 1994–2007: A comprehensive review of validation data and clinical results. Br J Dermatol 2008; 159(5):997–1035.
4. Guy AW. Biophysics of high-frequency currents and electromagnetic radiation. In: Lehmann JF, editor. Therapeutic heat and cold, 4th edition. Baltimore, MD: Williams and Wilkins; 1990. pp 179–236.
5. Guy AW. History of biological effects and medical applications of microwave energy. IEEE Trans Microw Theory Tech 1984;32(9):1182–1200.
6. Krusen FH. Samuel hyde memorial lecture: Medical applications of microwave diathermy: Laboratory and clinical studies. Proc R Soc Med 1950;43(8):641.
7. Johnson JE, Neumann DG, Maccarini PF, Juang T, Stauffer PR, Turner P. Evaluation of a dual-arm Archimedean spiral array for microwave hyperthermia. Int J Hyperthermia 2006;22(6):475–490.
8. Rosen A, Greenspon AJ, Walinsky P. Microwaves treat heart disease. IEEE Microw Mag 2007;8(1):70–75.
9. Stauffer PR. Thermal therapy techniques for skin and superficial tissue disease. In: Ryan TP, editor. A critical review, matching the energy source to the clinical need. Bellingham, WA: SPIE Optical Engineering Press; 2000. pp 327–367.
10. Stauffer PR. Evolving technology for thermal therapy of cancer. Int J Hyperthermia 2005;21(8):731–744.
11. Sterzer F. Microwave medical devices. IEEE Microw Mag 2002;3(1):65–70.
12. Vander Vorst A, Rosen A, Kotsuka Y. RF/microwave interaction with biological tissues. Hoboken, NJ: John Wiley & Sons, Inc.; 2006.
13. Pozar DM. Microwave engineering, 2nd edition. New York, NY: John Wiley & Sons. Inc.; 1998.
14. Gabriel C, Gabriel S, Grant EH, Halstead BSJ, Mingos DMP. Dielectric parameters relevant to microwave dielectric heating. Chem Soc Rev 1998;27(3):213–224.
15. Beer GM, Baumuller S, Zech N, Wyss P, Strasser D, Varga Z, Seifert B, Hafner J, Mihic-Probst D. Immunohistochemical differentiation and localization analysis of sweat glands in the adult human axilla. Plast Reconstr Surg 2006;117(6): 2043–2049.
16. Gandhi OP, Lazzi G, Furse CM. Electromagnetic absorption in the human head and neck for mobile telephones at 835 and 1900 MHz. IEEE Trans Microw Theory Tech 1996; 44(10):1884–1897.
17. Ross EV, McKinlay JR, Sajben FP, Miller CH, Barnette DJ, Meehan KJ, Chhieng NP, Deavers MJ, Zelickson BD. Use of a novel erbium laser in a yucatan minipig: A study of residual thermal damage, ablation, and wound healing as a function of pulse duration. Lasers Surg Med 2002;30(2):93–100.
18. Ross EV, Naseef GS, McKinlay JR, Barnette DJ, Skrobal M, Grevelink J, Anderson R. Comparison of carbon dioxide laser, erbium: Yag laser, dermabrasion, and dermatome a study of thermal damage, wound contraction, and wound healing in a live pig model: Implications for skin. Resurfacing. J Am Acad Dermatol 2000;42(1):92–105.
19. Ross EV, Yashar SS, Naseef GS, Barnette DJ, Skrobal M, Grevelink J, Anderson R. A pilot study of in vivo immediate tissue contraction with CO_2 skin laser resurfacing in a live farm pig. Dermatol Surg 1999;25(11):851–856.
20. Sullivan TP, Eaglstein WH, Davis SC, Mertz P. The pig as a model for human wound healing. Wound Repair Regen 2001;9(2):66–76.
21. Vardaxis NJ, Brans TA, Boon ME, Kreis RW, Marres LM. Confocal laser scanning microscopy of porcine skin: Implications for human wound healing studies. J Anat 1997;190(04): 601–611.
22. Gabriel C, Gabriel S, Corthout E. The dielectric properties of biological tissues: I. Literature survey. Phys Med Biol 1996; 41(11):2231–2249.
23. Gabriel S, Lau RW, Gabriel C. The dielectric properties of biological tissues: II. Measurements in the frequency range 10 Hz to 20 GHz. Phys Med Biol 1996;41(11):2251–2269.
24. Peyman A, Gabriel C. Cole-cole parameters for the dielectric properties of porcine tissues as a function of age at microwave frequencies. Phys Med Biol 2010;55(15):N413–N419.
25. Gabriel S, Lau RW, Gabriel C. The dielectric properties of biological tissues: III. Parametric models for the dielectric spectrum of tissues. Phys Med Biol 1996;41(11):2271–2293.